Journal of Materials Chemistry C

Accepted Manuscript

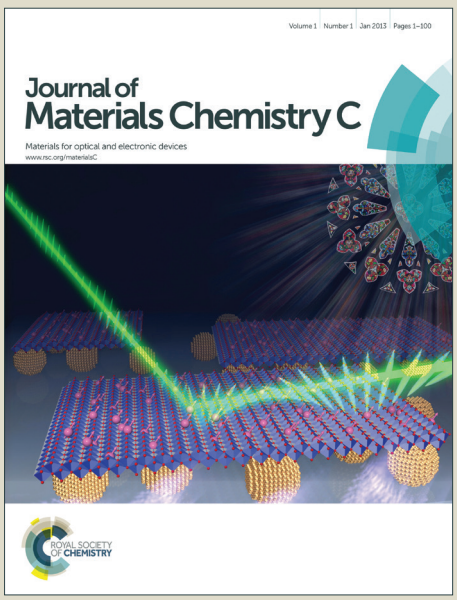

ROYAL SOCIETY OF CHEMISTRY

www.rsc.org/materialsC

Journal Name

ARTICLE

The Mg/W codoped Vanadium Dioxide Thin Films with Enhanced Visible Transmittance and Low Phase Transition Temperature

Received 00th January 20xx,
Accepted 00th January 20xx

DOI: 10.1039/x0xx00000x

www.rsc.org/

Ning Wang,[a] Shiyu Liu,[b] X.T. Zeng,[b] Shlomo Magdassi[c] and Yi Long*[a]

Vanadium dioxide (VO_2) with the reversible phase transition near to the ambient temperature has been found to be a promising candidate for energy-saving smart windows. However it is constrained by the low visible transmission (T_{lum}) and high transition temperature (τ_c). In this paper, by codoping tungsten (W) and magnesium (Mg) in VO_2, a good combination of low τ_c (~ 35 °C) and high T_{lum} (81.3%) was achieved. The τ_c declines with decreasing Mg doping level in Mg/W codoped samples, which is opposite to the single Mg doping, suggesting the synergistic effect of the two dopants arising from the e^- and h^+ carrier neutralization. In addition, the band gap of Mg/W codoped VO_2 was gradually widened, attributing to the depressed absorption and thus enhancing the T_{lum}.

Introduction

Vanadium dioxide (VO_2) has attracted intense interest since its metal to insulator transition (MIT) was reported in 1959.[1] As a reversible phase transition material, VO_2 exhibits a first-order transition from insulating monoclinic ($P2_1/c$, M-phase) to metallic rutile structure ($P4_2/mnm$, R-phase) across the critical temperature (τ_c, ~68 °C) [2] with abruptly depressed infrared (IR) transmittance and the unchanged visible transmission (T_{lum}), which makes it a promising candidate for thermochromic smart windows.[3-7] However, the relatively high τ_c above room temperature and the low T_{lum} due to large absorption and reflection largely restrict its energy saving efficiency. Recently, many efforts have been made to improve the T_{lum} and solar modulating ability (ΔT_{sol}) of VO_2,[5-6, 8-13] but the combination of low τ_c and high T_{lum} as well as large ΔT_{sol} is still challenging.

In order to reduce τ_c, great efforts have been made by the scientists, such as introducing strains into the crystal lattice[14-15] and doping (Table 1). During the MIT, the τ_c could be modified by the uniaxial stress σ following the Clausius-Clapeyron equation, $d\tau_c / d\sigma = (\varepsilon_0 \tau_c^0) / \Delta H$ (1), where ΔH is the latent heat of the transition, ε_0 is the initial strain and τ_c^0 is the initial phase transition temperature.[14] On the other hand, doping with higher valence-state cation (compared to V^{4+}) could result in the extra electrons, which can break the structural symmetry of VO_2 in terms of dimerization of V-V chain in the R-phase to reduce the energy difference between M- and R-phases, and thereby decreasing the τ_c.[16-18] In addition, the substitution of V^{4+} by cations with larger ionic radius or the insertion of cations at interstitial sites of the VO_2 lattice could introduce compressive strain and induce structure deformation which would also reduce the τ_c.[14, 19] Among the cations, W is the most efficient dopant to reduce τ_c with a rate of ~20-26 °C /at.% mainly owing to its high valence state (6+). However, the sharp decrease of τ_c arising from the W doping is always accompanied by the decline of T_{lum} and ΔT_{sol}.[20-21] Meanwhile, Mg^{2+} has been doped in VO_2 to enhance the T_{lum} of VO_2 thin films where the band gap is steadily widened upon doping, whilst the τ_c can only be reduced to 47 °C even at 7 at.% doping level.[22-23]

Table 1. Effects of dopants on the thermochromic performance of VO_2 thin films[a].

Dopant	T_{lum}	ΔT_{sol}	τ_c	Mechanism	Ref.
W^{6+}	↓	↓	↓(~20-26 °C/at.%)	e^-↑	20-21
Ti^{4+}	↑	↑	↑	smaller radius	24-25
Co^{2+}	–	–	↓	larger radius	26
Nb^{5+}	↓	↓	↓(~2 °C/at.%)	e^-↑	27
Mo^{6+}	↑	↓	↓(~3 °C/at.%)	e^-↑	27
Ta^{5+}	–	–	↓	e^-↑	26
Mg^{2+}	↑	↑	↓(~3 °C/at.%)	h^+↑	22-23
Zr^{4+}	↑	↑	↓(~0.4 °C/at.%)	larger radius	28
Cr^{3+}	↑	↓	↑	h^+↑	29
Sn^{4+}	–	–	↑(~1 °C/at.%)	smaller radius	30
Al^{3+}	–	–	↓(~2.7 °C/at.%)	h^+↑	31
Fe^{3+}	–	–	↓(~6 °C/at.%)	h^+↑	32
Eu^{3+}	↑	↑	↓(~5 °C/at.%)	larger radius	33
Ce^{3+}	–	–	↓(~4.5 °C/at.%)	larger radius	34

[a] In the table, '↓' and '↑' represent the reducing and improving effects of the dopants, respectively. The symbol '–' means Not Available.

Besides, the Mo/W[35-36] and Ti/W codoping[37] have been carried out to tune the τ_c of VO_2. The Mo/W codoped VO_2 thin films exhibited the interesting non-linear effect between the co- and

[a] School of Materials Science and Engineering, Nanyang Technological University, 50 Nanyang Avenue, 639798 Singapore. E-mail: longyi@ntu.edu.sg
[b] Singapore Institute of Manufacturing Technology, 71 Nanyang Drive, 638075 Singapore.
[c] Institute of Chemistry, Edmund Safra Campus, The Hebrew University, Jerusalem 91904, Israel..

Electronic Supplementary Information (ESI) available: [High resolution XPS scan of the samples]. See DOI: 10.1039/x0xx00000x

single-doping, where the τ_c lowering efficiency was enhanced compared with single doping. However, the mechanism of codoping was unclear and the influence on $T_{lum}/\Delta T_{sol}$ was not reported.[36] Ti/W codoping showed a higher τ_c than single W doping due to the decrease of carrier density arising from the electron transfer from W donor to Ti acceptor while the transmission was largely compromised compared with the pure VO_2.

In this paper, the Mg/W codoping has been carried out systematically to investigate the synergistic effect on the thermochromic properties of VO_2 thin films. The large τ_c reducing rate of W and the superior T_{lum} enhancing ability of Mg have been combined to give enhanced thermochromic properties. Possible mechanisms of such enhancement are discussed.

Experimental

All of the materials V_2O_5 (99.6%, Alfa Aesar), Mg, W powders (99.9%, Alfa Aesar), Polyvinylpyrrolidone (PVP40, Sigma-Aldrich), oxalic acid (99.9%, Alfa Aesar) and H_2O_2 (30 wt.%, Sigma-Aldrich) were used as received without any further purification.

Mg/W codoped precursor preparation. The precursor was prepared by a modified sol-gel method, details of which have been reported elsewhere.[38-40] Weighed Mg and W powders were dissolved in 15 mL preheated H_2O_2 solution (30 wt.%) at 90 °C with continuous stirring for 5 h. 180 mg of V_2O_5 powder was then added into the hot solution. After a vigorous reaction, 400 mg of oxalic acid was added to reduce the vanadium source from V^{5+} to V^{4+} with continuous stirring for two more hours at 90 °C. Ultimately, 12 mg of PVP was added into the solution and a blue colored solution precursor was formed. The amount of Mg and W powder was calculated based on the formula $V_{1-x-y}W_xMg_yO_2$ (x=0, 0.02; y=0, 0.01/0.02/0.03/0.04/0.05).

Vanadium dioxide thin film preparation. The precursor thin films were prepared by withdrawing the fused silica substrate (15×15×0.6mm^3) from the codoped precursor solution at the rate of 1000 mm/min using a *KSV* dip coater. After drying in air, the thin films were annealed in a tube furnace with Ar flow (200 cc/min) at 550 °C for 2 h and bronze colored thin films with the thickness ~50 nm were attained on both sides of the substrates.

Characterization. The phase of the obtained thin films were characterized with Shimadzu XRD-6000 X-Ray diffractometer (Cu-Kα, λ = 0.15406 nm) with a voltage of 40 kV and a current of 30 mA at an X-ray grazing angle of 1.0°. The surface topography was determined by the atomic force microscopy (AFM, DI-3100, Bruker, Germany) using tapping mode. The TEM characterization was performed with JEOL JEM 2010 with the accelerating voltage of 200 kV. The XPS data were collected in the V 2p, Mg 1s and W 4f binding energy regions using a Thermo Scientific ESCALAB 250Xi XPS spectrometer (900 μm spot, 3 scans, 75 eV pass energy) equipped with Avantage Data System software. The thickness of the VO_2 film was measured by Alpha-Step IQ Surface Profiler. The transmittance spectra in the range of 250-2500 nm was measured with a UV-Vis-NIR spectrophotometer (Cary 5000, Agilent Ltd) equipped with a Linkam PE120 system Peltier simple heating & cooling stage. The integrated visible transmittance (T_{lum}, 380-780 nm) and solar transmittance (T_{sol}, 280-2500 nm) were calculated based on the recorded %T spectra using the following expression:

$$T_{lum/sol}=\int\varphi_{lum/sol}(\lambda)T(\lambda)d\lambda/\int\varphi_{lum/sol}(\lambda)\,d\lambda \quad (2)$$

Where $T(\lambda)$ is the recorded film transmittance, φ_{lum} is the standard luminous efficiency function for the photopic vision of human eyes,[41] φ_{sol} is the solar irradiance spectrum for air mass 1.5 (corresponding to the sun standing 37˚ above the horizon)[42] and the ΔT_{sol} is obtained by $\Delta T_{sol} = T_{sol,15\,°C} - T_{sol,90°C}$. The hysteresis loop of %T at the wavelength of 2500 nm was measured at the temperature ranging from 10 to 90 °C. In order to attain the phase transition temperature τ_c, the temperature dependent heating and cooling %T data were fitted with a sigmoidal function in the form[43]

$$f(\tau)=A2+(A1-A2)/\{1+exp[(\tau-\tau_0)/B]\} \quad (3)$$

where $A1$, $A2$, τ_0 and B are fitting parameters with τ_0 giving the transition temperature in the heating and cooling cycle and $\tau_c = (\tau_{0,h}+\tau_{0,c})/2$, $\Delta\tau_c = \tau_{0,h}-\tau_{0,c}$.

Results and discussion

Synthesis of Mg/W codoped VO_2 thin films

Figure 1 shows the XRD results of the pristine and doped VO_2 samples. All of the XRD patterns show the characteristic (011) peak at around 2ϑ=28° for the monoclinic VO_2 phase ($P2_1/c$, JCPDS #82-661). No diffraction peaks of other vanadium oxide or magnesium/tungsten oxide phases can be found within the patterns suggesting the high purity of the VO_2 phase with Mg/W dopants in the crystal lattice. The broad hump around 2ϑ=20° should be ascribed to the diffraction background of the fused silica substrates.

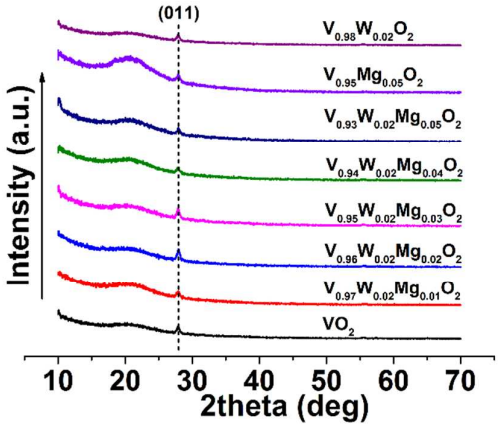

Figure 1. XRD patterns for the vanadium dioxide samples.

The topographical AFM images for the pristine and Mg/W codoped VO_2 thin films are shown in Figure 2. The AFM scan reveals that all of the VO_2 thin films have the densely packed nanograin-array topography with a narrow-distributed grain size below ~100 nm, which will greatly reduce the light scattering and enhance the T_{lum}.[44] The mean grain size of all the pristine VO_2 and co-doped samples ranges from 60-80 nm,

while that for single Mg doped VO_2 is approximately 50 nm. Since the grain sizes for doped and undoped samples do not vary significantly, the grain size effect on thermochromic properties could be negligible.

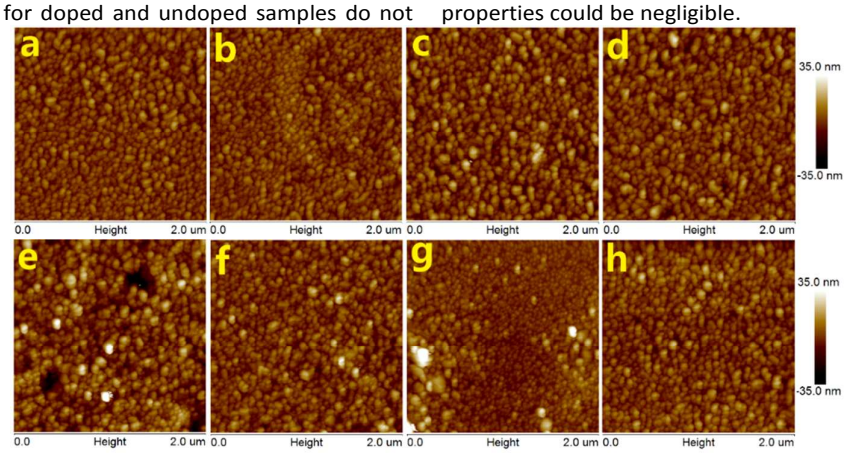

Figure 2. AFM images for the vanadium dioxide samples (a: pristine VO_2; b-f: $V_{0.98-x}W_{0.02}Mg_xO_2$, x=0.01/0.02/0.03/0.04/0.05; g: $V_{0.95}Mg_{0.05}O_2$; h: $V_{0.98}W_{0.02}O_2$) with the scanning scale 2×2 μm^2.

The bright-field TEM image of $V_{0.94}W_{0.02}Mg_{0.04}O_2$ is shown in Figure 3. The HRTEM image shows that the grains are well crystallized (Figure 3b) with a sub-100 nm grain size (Figure 3a) in accordance with the AFM results. The selected area electron diffraction (SAED) patterns as shown in Figure 3c can be indexed with VO_2(M) crystalline faces from (011) to (220), which reveals the polycrystalline nature of the thin film and further supports the high purity of the formed VO_2(M) phases as shown in XRD results.

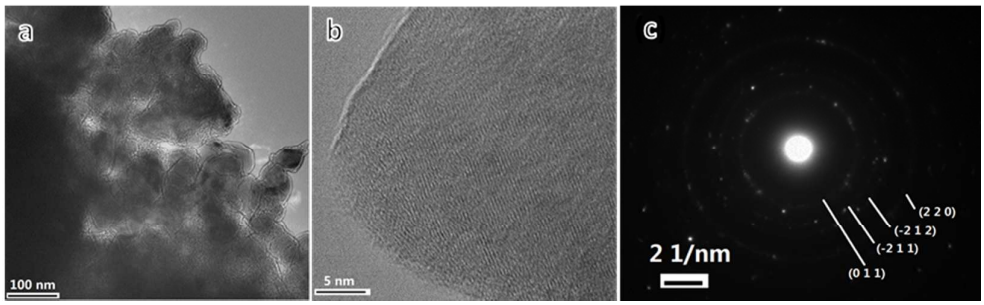

Figure 3. (a) Transmission electron microscopy (TEM), (b) HRTEM and (c) *Selected area electron diffraction* (SAED) images for the $V_{0.94}W_{0.02}Mg_{0.04}O_2$ sample.

The XPS scan for the Mg/W codoped VO_2 thin films was performed in the respective binding energy regions for V2p, Mg1s and W4f. As demonstrated in Figure S1, under every doping levels, the V2p1/2, V2p3/2 peaks for V2p scan, the Mg1s peak for Mg1s scan and the W4f5/2 and W4f7/2 peaks for W4f scan can all be clearly observed, proving the successful incorporation of Mg and W dopants into the VO_2 lattice since no Mg/W compounds could be indexed in the XRD patterns (Figure 1). In addition, the quantitative analysis reveals that the doping levels ($c_{Mg/W}/c_V$) detected by XPS are nearly the same as expected from the precursor solution (Table 2). As shown in Figure S1 a-e, for the V2p scan the V2p3/2 peak can be split into two peaks (V^{4+} around 516 eV and V^{3+} around 514 eV), which suggests the non- stoichiometry in the VO_2 phase. It is of interest that upon increasing the Mg doping levels from 1 to 5 at.%, the relative intensity of V^{3+} compared to V^{4+} is gradually depressed (Figure 4), in accord with the decrease of free electrons under the coexistence of Mg/W dopant due to the counteraction between the h^+ and e^- charge carriers.

Journal Name

ARTICLE

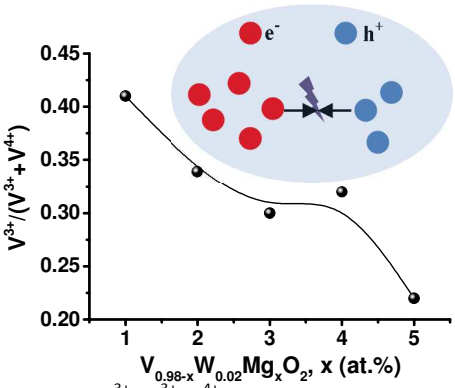

Figure 4. Ratio of $V^{3+}/(V^{3+}+V^{4+})$ for $V_{0.98-x}W_{0.02}Mg_xO_2$ samples.

Table 2. Doping level and stoichiometry of the Mg/W codoped VO_2 samples

Samples	Doping level of Mg, W ($c_{Mg/W}/c_V$)		Vanadium/ oxygen content	Stoichiometry
	Expected (at.%)	XPS result (at.%)	XPS result (at.%)	$V^{3+}/(V^{3+}+V^{4+})$
$V_{0.98}W_{0.02}O_2$	0.0, 2.0	0.0, 2.1	18.2/78.8	0.45
$V_{0.95}Mg_{0.05}O_2$	5.0, 0.0	5.0, 0.0	13.4/83.2	0.16
$V_{0.97}W_{0.02}Mg_{0.01}O_2$	1.0, 2.0	1.2, 1.8	27.2/67.7	0.41
$V_{0.96}W_{0.02}Mg_{0.02}O_2$	2.0, 2.0	1.9, 2.1	22.5/72.1	0.34
$V_{0.95}W_{0.02}Mg_{0.03}O_2$	3.0, 2.0	2.7, 1.9	17.1/80.2	0.30
$V_{0.94}W_{0.02}Mg_{0.04}O_2$	4.0, 2.0	3.8, 1.8	14.7/75.6	0.32
$V_{0.93}W_{0.02}Mg_{0.05}O_2$	5.0, 2.0	5.3, 2.1	13.3/77.5	0.22

Optical properties

The UV-Vis-NIR transmittance spectra for the VO_2 thin films were recorded at 15 and 90 °C, respectively (Figure 5a). A drop in the transmission was observed for all of the samples above the wavelength of 1000 nm upon heating from 15 to 90 °C, in accordance with the intrinsic MIT characteristics of VO_2. Among the samples, the single Mg doped $V_{0.95}Mg_{0.05}O_2$ shows the highest solar transmission in the whole spectrum (250-2500 nm) at both temperatures, especially in the visible range indicating the enhancing ability of Mg in T_{lum}. On the contrary, the single W doped $V_{0.98}W_{0.02}O_2$ gives the lowest solar transmission (250-2500 nm) uncovering the weakness of W as a dopant. Meanwhile, on the basis of 2 at.% W doping, the further codoping with Mg effectively improves T_{lum} and the solar transmission compared with single W doping and gives the closest result to single Mg doping at the doping level of 4 at.% ($V_{0.94}W_{0.02}Mg_{0.04}O_2$), which can be confirmed by the calculated T_{lum} and ΔT_{sol}. (Table 3). Figure 5b shows the reflection (%R) and absorption (%A) spectra of the thin films, where the %A was calculated from 1-%R-%T. All of the %R at λ=580 nm fall into the range 14.9-17.8%. Single W doping gives highest absorption from 380-2500 nm which suggests that W doping increases the absorption coefficient of VO_2, which largely contributes to depressed T_{lum} (Table 3); meanwhile, single Mg doping gives the lowest absorption over most of the wavelengths which proves that Mg doping largely reduces the absorption coefficient of VO_2.[22, 45] Compared with 2 at.% W single doping, the codoping with Mg decreases the %A (λ=580 nm) and the lowest absorption is again attained at the doping level of 4 at.% ($V_{0.94}W_{0.02}Mg_{0.04}O_2$) attributing to its high T_{lum} as observed in the %T spectra (Figure 5a and Table 3).

Journal Name

ARTICLE

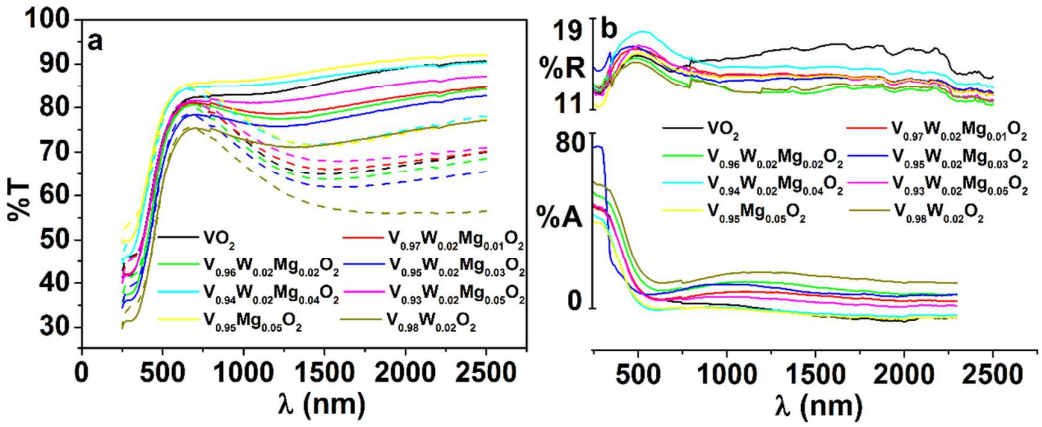

Figure 5. (a) Transmittance spectra in the UV-Vis-NIR range for the vanadium dioxide samples. The solid and dash lines represent the spectra tested at 15 °C and 90 °C, respectively. (b) Recorded %R and %A spectra for the pristine and Mg/W codoped VO_2 samples.

The calculated average T_{lum} [($T_{lum,\ 15°C}$+ $T_{lum,\ 90°C}$)/2] and ΔT_{sol} ($T_{sol,\ 15°C}$-$T_{sol,\ 90°C}$) for the pristine and codoped VO_2 thin films are listed in Table 3. As shown in Table 3, compared with the pristine VO_2, the single 5 at.% Mg doping is found to enhance the average T_{lum} from 77.5% to 82.1%, whilst the sole 2 at.% W doping reduces it to 69.5%. Based on the 2 at.% W dopings, the further doping with Mg recovers the average T_{lum} above 70% and the highest value 81.3% is reached at 4 at.% Mg doping ($V_{1.94}W_{0.02}Mg_{0.04}O_2$) proving that the ability of Mg doping in enhancing the T_{lum} is maintained with codoping of W.

Table 3. Thermochromic performance of the pristine, single and codoped VO_2 thin films.

Sample	%R(580nm)	%A(580nm)	Average T_{lum}/%	ΔT_{sol}/%	τ_c/°C	$\Delta\tau_c$/°C	E_g^*/eV
VO_2	15.6	5.0	77.5	5.9	63.89	19.8	2.88
$V_{0.98}W_{0.02}O_2$	14.9	13.5	69.5	3.4	27.05	8.7	2.67
$V_{0.95}Mg_{0.05}O_2$	15.9	0.6	82.1	4.8	61.05	16.7	2.99
$V_{0.97}W_{0.02}Mg_{0.01}O_2$	16.2	5.2	77.0	3.3	30.45	8.7	2.83
$V_{0.96}W_{0.02}Mg_{0.02}O_2$	16.0	8.9	76.0	3.9	29.55	7.9	2.72
$V_{0.95}W_{0.02}Mg_{0.03}O_2$	16.0	5.7	73.3	3.7	32.55	8.5	2.75
$V_{0.94}W_{0.02}Mg_{0.04}O_2$	**17.8**	**0.0**	**81.3**	**4.3**	**35.05**	**8.9**	**3.02**
$V_{0.93}W_{0.02}Mg_{0.05}O_2$	16.5	4.6	77.4	3.7	35.08	8.3	2.83

* The calculation errors for E_g is within 10%.

With regard to the phase transition temperature, the transmittance at the wavelength 2500 nm in the temperature range 10 to 90 °C was recorded in a heating and cooling cycle, and has been plotted as %T versus T/°C hysteresis loops (Figure 6a). Single Mg doping gives the highest IR transmission while single W doping presents the lowest IR transmission at different temperatures. As shown in Table 3, the pristine VO_2 exhibits the largest τ_c =63.9 °C and the widest $\Delta\tau_c$ =19.8 °C. It is of interest that the τ_c of the pristine VO_2 is much lower than the reported value 68-70 °C, which should mainly be due to its sub-100 nm grain size (Figure 2), and the nanograin size effect should also contribute to its widened hysteresis loop width $\Delta\tau_c$ (19.8 °C) compared to the bulk counterparts.[46] Compared to the pristine sample, the single doping samples with 5 at.% Mg and 2 at.% W reduce the τ_c to 61.05 °C and 27.05 °C while narrowing down the $\Delta\tau_c$ to 16.7 °C and 8.7 °C, respectively, which are comparable to the reported values.[20, 22] The much sharper reduction of τ_c and $\Delta\tau_c$ under the W doping should be mainly owing to the high valence state of the W^{6+} introducing free electrons to the V^{4+} cation. When it turns to Mg/W codoping, a τ_c increasing tendency is found (Figure 6b), where the continuous Mg doping under the pre-existence of 2 at.% W dopant results in a slight increase of τ_c from 27.05 °C ($V_{0.98}W_{0.02}O_2$) to 35.08 °C ($V_{0.93}W_{0.02}Mg_{0.05}O_2$) at a rate of 1.6 °C/at.%. As reported in literature, doping with cations with higher/lower valence state in VO_2 lattice could result in the free electron (e^-)/hole (h^+) charge carriers, and create the V^{3+}/V^{5+} defect sites, respectively.[16] The coexistence of W and Mg dopant in the VO_2 lattice may decrease the free charge carrier density arising from the e^- and h^+ charge carriers

combination, which should be responsible for the increased τ_c under codoping conditions since τ_c is closely linked to the equilibrium carrier density.[47]

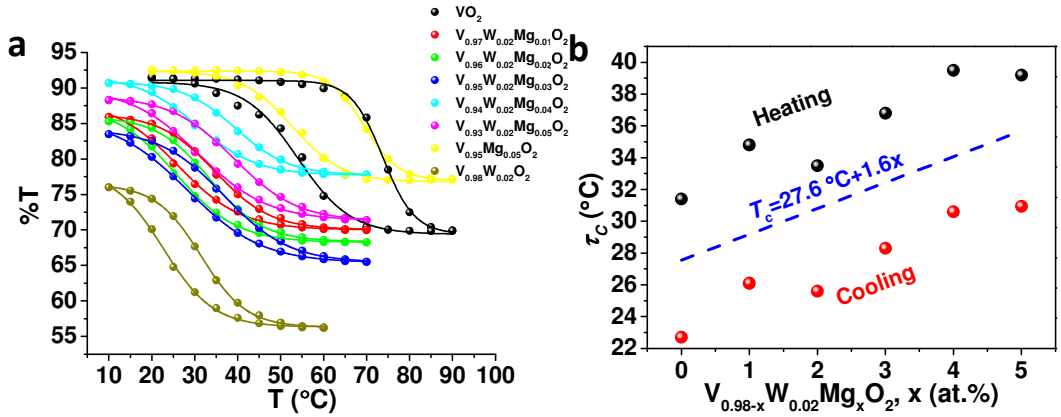

Figure 6. (a) Hysteresis loop for the temperature dependent transmittance of the VO_2 samples at the wavelength 2500 nm and (b) the plots of doping dependent τ_c. The solid lines in (a) represent the best fitting results as described in the text.

As reported by Li. et al.,[22] the Mg doping could increase the band gap of the vanadium dioxide. Herein, the band gap E_g of the pristine and doped VO_2 samples is determined by fitting the linear part of the curve $(\alpha\hbar\omega)^2$ versus $\hbar\omega$ (Figure 7a) with the expression

$$(\alpha\hbar\omega)^2 = A(\hbar\omega - E_g) \quad (4)$$

where α is the absorption coefficient (αd=-ln(T/1-R)), A is a constant and $\hbar\omega$ is the photon energy. The best fitting result has been tabulated in Table 3, where E_g is increased from 2.88 (pristine VO_2) to 2.99 eV ($V_{0.95}Mg_{0.05}O_2$) under sole doping of Mg, in accordance with the band gap widening effect of Mg reported by Li. et al.[22] Under Mg/W-codoping conditions ($V_{0.98-x}W_{0.02}Mg_xO_2$), the E_g is also widened upon Mg doping, and approximately follows the increasing rate of 0.04 eV/at.% (inset in Figure 7b). It is of interest that E_g exhibits a similar trend across the doping levels to that of average T_{lum}. The T_{lum} versus E_g has been plotted in Figure 7b, and a positive linear relationship between T_{lum} and E_g can be clearly concluded, which should be attributed to the steady decrease of the absorption along with the widened band gap E_g.

In summary, the Mg/W codoping can assist the combination of high T_{lum} and low τ_c, superior to the single W or Mg doping since they have the obvious weakness in maintaining the high T_{lum} and reducing the τ_c, respectively. It should be of great significance for the smart window applications of VO_2 thin films.

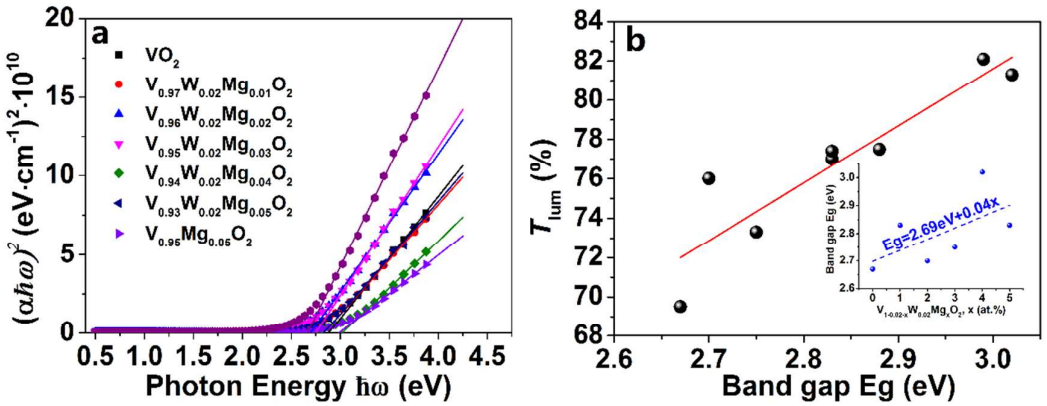

Figure 7. $(\alpha\hbar\omega)^2$ versus $\hbar\omega$, where α is the absorption coefficient and $\hbar\omega$ is the photon energy, with linear fittings to extract bandgap E_g at α=0 (a) and the relationship between the average T_{lum} and E_g (b). The solid line in (b) is a linear fit. The inset in (b) is plots of Mg doping dependent E_g under Mg/W-codoping conditions.

Conclusions

In summary, Mg/W codoped VO_2 thin films can benefit from both the τ_c lowering property of W and the T_{lum} increasing property of Mg. The τ_c under W/Mg codoping is found to be increasing at the rate of 1.6 °C/at.% upon increasing Mg

doping levels, which should be due to the decline of carrier density arising from the counteraction between e^- and h^+ carriers. The band gap widening effect in the single Mg dopant remains in codoped samples, leading to enhanced T_{lum}. The best performing sample $V_{0.94}W_{0.02}Mg_{0.04}O_2$ exhibits low τ_c (~30 °C) as well as high T_{lum} (~80%), which is of great practical significance in smart window applications.

Acknowledgements

This research is supported by the Singapore National Research Foundation under CREATE programme: Nanomaterials for Energy and Water Management and Singapore Ministry of Education (MOE) Academic Research Fund Tier 1 RG101/13. The XRD, FESEM and TEM characterizations were performed at the Facility for Analysis, Characterization, Testing and Simulation (FACTS) in Nanyang Technological University, Singapore. We also thank Mr. Min hao Goh for XPS characterization.

References

1 F. Morin, *Phys. Rev. Lett.*, 1959, 3, 34-36.
2 S. Biermann, A. Poteryaev, A. Lichtenstein and A. Georges, *Phys. Rev. Lett.*, 2005, 94, 026404.
3 M. E. A. Warwick and R. Binions, *J. Mater. Chem. A*, 2014, 2, 3275-3292.
4 Y. Gao, H. Luo, Z. Zhang, L. Kang, Z. Chen, J. Du, M. Kanehira and C. Cao, *Nano Energy*, 2012, 1, 221-246.
5 X. Qian, N. Wang, Y. Li, J. Zhang, Z. Xu and Y. Long, *Langmuir*, 2014, 30, 10766-10771.
6 X. Cao, N. Wang, J. Y. Law, S. C. J. Loo, S. Magdassi and Y. Long, *Langmuir*, 2014, 30, 1710-1715.
7 C. Liu, I. Balin, S. Magdassi, I. Abdulhalim and Y. Long, *Opt. Express*, 2015, 23, A124-A132.
8 Y. Zhou, Y. Cai, X. Hu and Y. Long, *J. Mater. Chem. A*, 2015, 3, 1121-1126.
9 Y. Zhou, Y. Cai, X. Hu and Y. Long, *J. Mater. Chem. A*, 2014, 2, 13550-13555.
10 L. Kang, Y. Gao, H. Luo, Z. Chen, J. Du and Z. Zhang, *ACS Appl. Mater. Interfaces*, 2011, 3, 135-138.
11 Y. F. Gao, S. B. Wang, H. J. Luo, L. Dai, C. X. Cao, Y. L. Liu, Z. Chen and M. Kanehira, *Energy Environ. Sci.*, 2012, 5, 6104-6110.
12 Z. Chen, C. Cao, S. Chen, H. Luo and Y. Gao, *J. Mater. Chem. A*, 2014, 2, 11874-11884.
13 Z. Chen, Y. Gao, L. Kang, C. Cao, S. Chen and H. Luo, *J. Mater. Chem. A*, 2014, 2, 2718-2727.
14 J. Cao, E. Ertekin, V. Srinivasan, W. Fan, S. Huang, H. Zheng, J. W. L. Yim, D. R. Khanal, D. F. Ogletree, J. C. Grossmanan and J. Wu, *Nat. Nanotechnol.*, 2009, 4, 732-737.
15 Y. Gu, J. Cao, J. Wu and L.-Q. Chen, *J. Appl. Phys.*, 2010, 108, 083517.
16 J. B. Goodenough, *J. Solid State Chem.*, 1971, 3, 490-500.
17 P. Kiri, G. Hyett and R. Binions, *Advanced Materials Letters*, 2010, 1, 86-105.
18 J. Zhang, H. He, Y. Xie and B. Pan, *J. Chem. Phys.*, 2013, 138, 114705-114706.
19 J. Zhang, H. He, Y. Xie and B. Pan, *Phys. Chem. Chem. Phys.*, 2013, 15, 4687-4690.
20 A. Romanyuk, R. Steiner, L. Marot and P. Oelhafen, *Sol. Energy Mater. Sol. Cells*, 2007, 91, 1831-1835.
21 R. Binions, C. Piccirillo and I. P. Parkin, *Surf. Coat. Technol.*, 2007, 201, 9369-9372.
22 S.-Y. Li, N. R. Mlyuka, D. Primetzhofer, A. Hallén, G. Possnert, G. A. Niklasson and C. G. Granqvist, *Appl. Phys. Lett.*, 2013, 103, 161907.
23 N. R. Mlyuka, G. A. Niklasson and C. G. Granqvist, *Appl. Phys. Lett.*, 2009, 95, 171909.
24 S. Chen, L. Dai, J. Liu, Y. Gao, X. Liu, Z. Chen, J. Zhou, C. Cao, P. Han, H. Luo and M. Kanahira, *Phys. Chem. Chem. Phys.*, 2013, 15, 17537-17543.
25 J. Du, Y. Gao, H. Luo, L. Kang, Z. Zhang, Z. Chen and C. Cao, *Sol. Energy Mater. Sol. Cells*, 2011, 95, 469-475.
26 K. Isamu and W. Akinori, *Jpn. J. Appl. Phys.*, 1967, 6, 1023.
27 C. Batista, R. M. Ribeiro and V. Teixeira, *Nanoscale Res. Lett.*, 2011, 6, 301.
28 N. Shen, S. Chen, Z. Chen, X. Liu, C. Cao, B. Dong, H. Luo, J. Liu and Y. Gao, *J. Mater. Chem. A*, 2014, 2, 15087-15093.
29 F. Béteille and J. Livage, *J. Sol-Gel Sci. Technol.*, 1998, 13, 915-921.
30 M.-H. Lee, M.-G. Kim and H.-K. Song, *Thin Solid Films*, 1996, 290–291, 30-33.
31 B. Chen, D. Yang, P. A. Charpentier and M. Zeman, *Sol. Energy Mater. Sol. Cells*, 2009, 93, 1550-1554.
32 T. E. Phillips, R. A. Murphy and T. O. Poehler, *Mat. Res. Bull.*, 1987, 22 1113-1123.
33 X. Cao, N. Wang, S. Magdassi, D. Mandler and Y. Long, *Sci. Adv. Mater.*, 2014, 6, 558-561.
34 L. Song, Y. Zhang, W. Huang, Q. Shi, D. Li, Y. Zhang and Y. Xu, *Mater. Res. Bull.*, 2013, 48, 2268-2271.
35 Y. Xu, W. Huang, Q. Shi, Y. Zhang, L. Song and Y. Zhang, *J. Sol-Gel Sci. Technol.*, 2012, 64, 493-499.
36 Y. Jiazhen, Z. Yue, H. Wanxia and T. Mingjin, *Thin Solid Films*, 2008, 516, 8554-8558.
37 M. Soltani, M. Chaker, E. Haddad, R. V. Kruzelecky and J. Margot, *Appl. Phys. Lett.*, 2004, 85, 1958.
38 N. Wang, S. Magdassi, D. Mandler and Y. Long, *Thin Solid Films*, 2013, 534, 594-598.
39 N. Wang, Y. Huang, S. Magdassi, D. Mandler, H. Liu and Y. Long, *RSC Adv.*, 2013, 3, 7124-7128.
40 C. Liu, N. Wang and Y. Long, *Appl. Surf. Sci.*, 2013, 283, 222-226.
41 G. Wyszecki and W. S. Stiles, *Color Science: Concepts and Methods, Quantitative Data and Fomulae*, Wiley, New York, Second edn., 2000.
42 ASTM G173-03 Standard Tables of Reference Solar Spectral Irradiances: Direct Normal and Hemispherical on a 37° Tilted Surface, Annual Book of ASTM Standards, American Society for Testing and Materials, Philadelphia, PA, USA, 2003, Vol. 14.04, http://rredc.nrel.gov/solar/spectra/am1.5.
43 G. Beydaghyan, V. Basque and P. V. Ashrit, *Thin Solid Films*, 2012, 522, 204-207.
44 J. Zhou, Y. Gao, Z. Zhang, H. Luo, C. Cao, Z. Chen, L. Dai and X. Liu, *Sci. Rep.*, 2013, 3, 3029.
45 Y. F. Gao, *Phys. Chem. Chem. Phys.*, 2013, 15, 7505-7511.
46 H. Verleur, A. Barker and C. Berglund, *Phys. Rev.*, 1968, 172, 788-798.
47 J. Wei, Z. Wang, W. Chen and D. H. Cobden, *Nat Nano*, 2009, 4, 420-424.

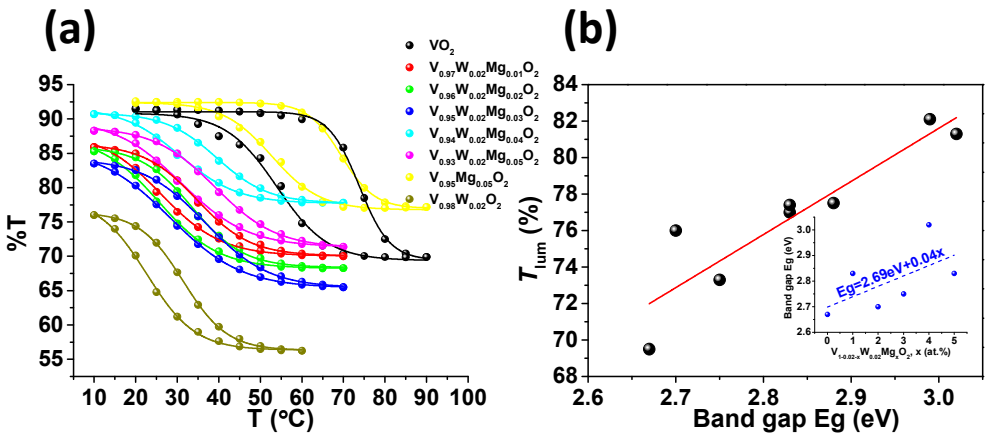

The Mg^{2+} and W^{6+} cations were firstly codoped into the VO_2 lattice, which gave rise to the photon band gap widening and h^+/ e^- charge carrier accumulation, attributing to enhancing of thermochromic performance with high visible transmission (~80%) and low phase transition temperature (~30 °C).